ELSEVIER

Technical Note

Investigation of thermal performance of solar air heater having roughness elements as a combination of inclined and transverse ribs on the absorber plate

Varun[a] , R.P. Saini[b] , S.K. Singal[b],*

[a]*NIT Hamirpur, India*
[b]*Alternate Hydro Energy Centre, Indian Institute of Technology, Roorkee, India*

Abstract

An experimental investigation has been carried out to study the heat transfer and friction characteristics by using a combination of inclined as well as transverse ribs on the absorber plate of a solar air heater. The experimental investigation encompassed the Reynolds number (Re) ranges from 2000 to 14 000, relative roughness pitch (p/e) 3–8 and relative roughness height (e/D_h) 0.030. The effect of these parameters on the heat transfer coefficient and friction factor has been discussed in the present paper and correlations for Nusselt number and friction factor has been developed within the reasonable limits. A procedure to compute the thermal efficiency based on heat transfer processes in the system is also given and the effect of these parameters on thermal efficiency has been discussed.
© 2007 Elsevier Ltd. All rights reserved.

Keywords: Roughness element; Nusselt number; Friction factor; Thermal efficiency

1. Introduction

Solar collectors (air heaters) for utilization of solar thermal energy are widely used in various equipments. Solar collectors have low thermal efficiency because of low convective heat transfer coefficient between the air and the absorber plate which leads higher temperature to the absorber plate which causes maximum thermal losses to the environment [1]. It has been found that the main thermal resistance to the convective heat transfer is due to the formation of boundary layer on the heat transferring surface. Efforts for increasing heat transfer have been directed towards artificially destroying or disturbing this boundary layer. The use of artificial roughness on a surface is an effective technique to enhance heat transfer to fluid flowing in the duct. Artificial roughness in the form of wires and in various arrangements has been used to create turbulence near the wall or to break the boundary layer [2]. Thus, the

artificial roughness can be employed for the enhancement of heat transfer coefficient between the absorber plate and air, improving the thermal performance of solar air heater. Contrary to this, the excessive disturbance to the boundary layer creates more friction resulting in more pumping power. Therefore, the turbulence must be created in the region of laminar sub layer. Sufficient information is available in the literature about heat transfer and friction characteristics for flow in roughened circular tubes and channels in the turbulent flow. The roughness wire orientation and geometry, i.e., pitch (p/e) and relative roughness height (e/D_h) strongly affects the flow structure [3–5].

In the present experimental study, a combination of transverse and inclined ribs used as roughness geometry on the absorber plate is taken, the range of parameters covered are Reynolds number (Re) 2000–14 000, pitch of ribs (p) 5–13 mm, roughness height (e) 1.6 mm and aspect ratio (W/H) of 10.

2. Experimental set-up

A schematic diagram of the experimental set-up is shown in Fig. 1. The duct consists of entry section, a test section

*Corresponding author. Tel.: +91 1332 285167; fax: +91 1332 273517.
E-mail addresses:* sunilfah@iitr.ernet.in, sunilksingal@gmail.com
(S.K. Singal).

Nomenclature

A_c	area of absorber plate (m^2)
A_o	throat area of orifice plate (m^2)
B_0	constant
C_d	coefficient of discharge for orificemeter
C_p	specific heat of air (J/kg K)
C_0	constant
D_h	hydraulic diameter of duct (m)
e	height of roughness element (m)
e/D_h	relative roughness height (dimensionless)
f	friction factor for roughened duct (dimensionless)
f_s	friction factor for smooth duct (dimensionless)
F_R	heat removal factor (dimensionless)
F'	collector-efficiency factor (dimensionless)
F_o	heat removal factor referred to the outlet temperature (dimensionless)
G	mass velocity (kg/s m^2)
h_w	wind convection coefficient (W/m^2 K)
h	average convective heat transfer coefficient (W/m^2 K)
H	height of duct (m)
I	insolation (W/m^2)
k	thermal conductivity of air (W/m K)
k_i	thermal conductivity of insulating material (W/m K)
L	test length (m)
m	mass flow rate of air (kg/s)
N	number of glass cover
Nu	Nusselt number of roughened duct (dimensionless)

Nu_s	Nusselt number of smooth duct (dimensionless)
p	rib pitch (m)
p/e	relative roughness pitch (dimensionless)
Pr	Prandtl number (dimensionless)
ΔP	pressure drop across the test length (Pa)
ΔP_o	pressure drop across the orifice meter (Pa)
q_u	rate of heat transfer to air (W)
Re	Reynolds number (dimensionless)
T	thickness of insulating material (m)
t_a	average temperature of air (°C)
t_i	average inlet temperature of air (°C)
t_o	average outlet temperature of air (°C)
t_p	average temperature of absorber plate (°C)
U_L	loss coefficient (W/m^2 K)
U_t	top loss coefficient (W/m^2 K)
v	velocity of air in the duct (m/s)
W	width of duct (m)
W/H	aspect ratio (dimensionless)

Greek symbols

$\langle\tau\alpha\rangle$	transmittance–absorptance product
β	ratio of orifice diameter to pipe diameter
ρ	density of air (kg/m^3)
θ	tilt angle of U-tube manometer
μ	dynamic viscosity (kg/m s)
σ	Stefan–Boltzman constant
ε_g	emittance of glass
ε_p	emittance of plate
η	thermal efficiency

and an exit section. The size of the entire duct is 2440 mm × 290 mm × 29 mm, out of which 1000 mm is the length of the test section. The entry and exit lengths are 900 and 540 mm, respectively. The entry and exit lengths are taken on the basis of ASHRAE standards 93-77 [6] which suggest minimum entry and exit lengths of $5\sqrt{WH}$ and $2.5\sqrt{WH}$, respectively, for the turbulent flow regime. An electric heater having identical dimensions as those of absorber plate is fabricated by combining series and parallel loops of Nichrome wire on asbestos sheet. The heat flux may be varied from 0 to 1000 W/m^2 by a variable transformer across it. A mica sheet of 1 mm is placed between the electric heater and absorber plate made of G I sheet (18 SWG). This mica sheet acts as an insulator between the electric heater and absorber plate. A 4 mm thick asbestos sheet followed by 20 mm thick layer of glass wool and 8 mm thick wood insulates the top of the heater assembly. The heater is placed 25 mm above the roughened absorber plate with the help of wooden spacers. Thus the heat is transferred from the heater assembly to the absorber plate mainly through radiation. The upper side of the absorber plate is painted black to facilitate the transfer of

heat. The roughness is produced by gluing the desired size of aluminum wires on the underside of the absorber plate. The lay-out of wire ribs on the absorber plate is shown in Fig. 2. At the end of duct, a plenum was provided to connect the rectangular duct with circular pipe.

Ambient air is sucked through the duct by means of a centrifugal blower driven by 1.5 kW, three phase, 230 V and 2820 rpm motor. Two gate valves, one on the inlet side and other on the outlet side of the blower are provided for precise control of the air flow rate through the system.

2.1. Instrumentation

(i) *Temperature measurement*: Calibrated copper-constantan (28 SWG), thermocouples were used for air and absorber plate temperature measurements. Fifteen thermocouples were mounted on the top side of absorber plate, as shown in Fig. 3, to measure the average temperature of the absorber plate. Six thermocouples were inserted at equal distance along the length of the test section duct to measure the average temperature of air while flowing through the test section. All thermocouples were connected to digital

1. AIR INLET
2. ENTRY SECTION
3. TEST SECTION
4. EXIT SECTION
5. PLENUM
6. ORIFICE METER
7. U-TUBE MANOMETER
8. MS PIPE
9. AIR OUTLET
10. CENTRIFUGAL BLOWER
11. MOTOR
12. VARIAC
13. SELECTOR SWITCH
14. DIGITAL MULTIMETER
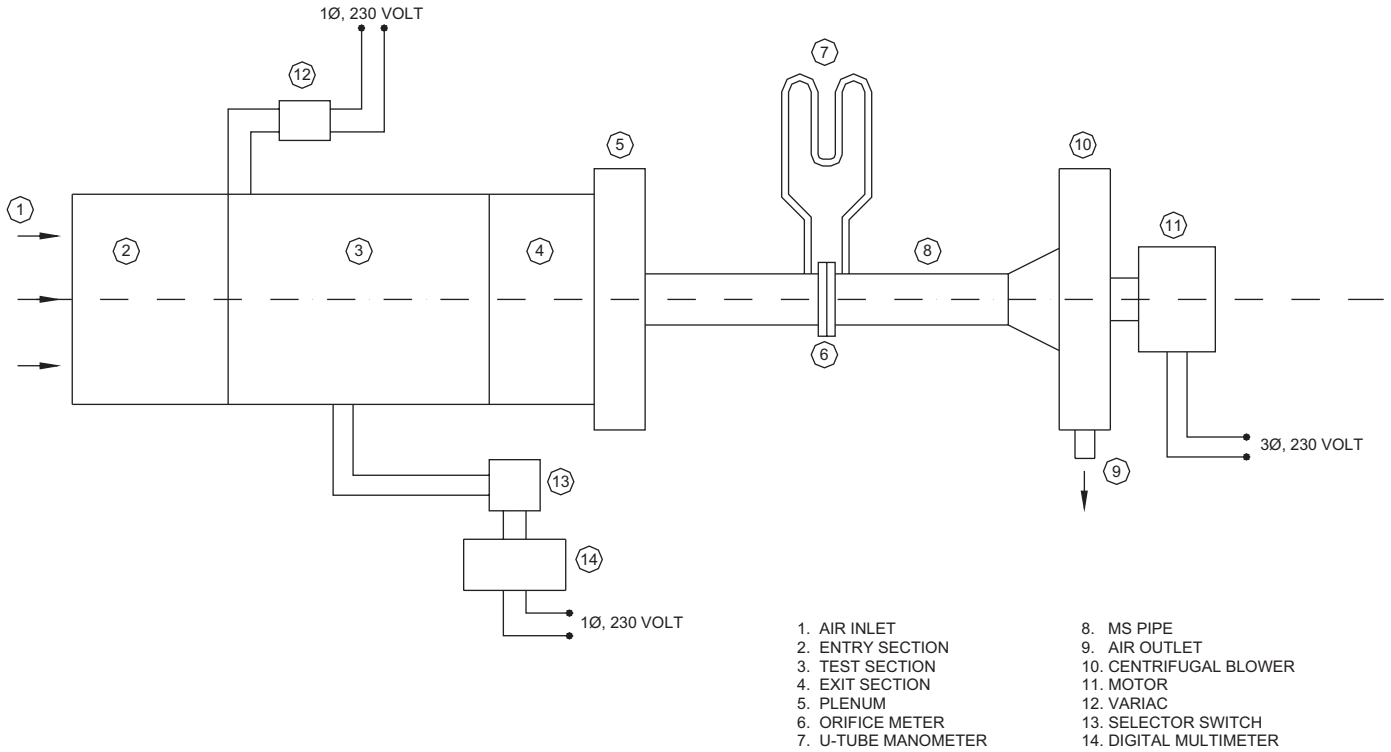
Fig. 1. Schematic diagram of experimental set-up.
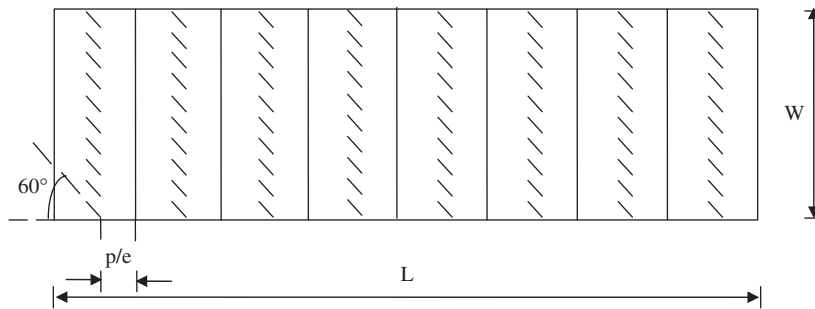
Fig. 2. Absorber plate showing the roughness element.

ALL DIMENSIONSARE IN MM.
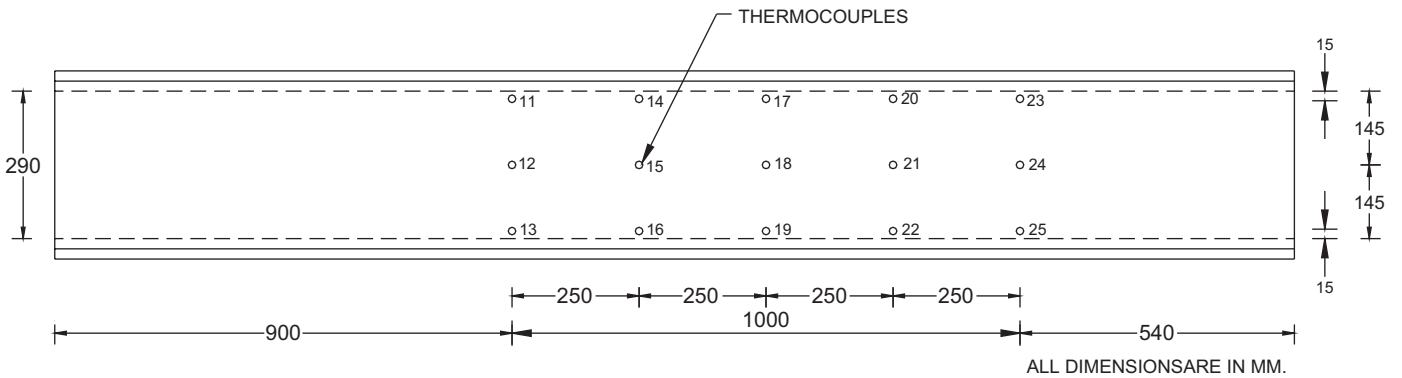
Fig. 3. Locations of thermocouple on absorber plate.

multimeter through a selector switch so that the output could be measured in °C.

(ii) *Air flow rate measurement*: The rate of air flow through the duct was measured by a flange type orifice meter which was designed, fabricated and fitted in the 81 mm diameter pipe carrying air from the plenum to the blower. The orifice meter was calibrated by using a pitot tube and the value of the coefficient of discharge was

obtained and used for calculating the flow rate of air. Pressure drop across the orifice meter was measured by means of a 10° inclined U-tube manometer.

(iii) *Pressure drop measurement*: The pressure drop across the test section of the duct was measured by means of a micro manometer having a least count of 0.01 mm. The micro manometer consists of a movable reservoir, a fixed reservoir and a transparent tube connected to these reservoirs through flexible tubing. The movable reservoir is mounted on a sliding arrangement using a lead screw having a pitch of 0.5 mm and a graduated dial having 50 divisions; each division showing a movement of 0.01 mm of the reservoir. The two reservoirs were connected with the air taps of the duct through flexible tubes. The meniscus is maintained at fixed prescribed mark by moving the reservoir up or down and movement is noted which yields the pressure difference across the two pressure tapings.

2.2. Experimental procedure

The set up runs to collect the data for heat transfer and friction factor under quasi-steady conditions. The power supply to the centrifugal blower and the electric heater was switched on and the desired flow rate was set with the help of control valves. In order to ensure the arrival of quasi-steady state conditions the values of temperature indicated by all the thermocouples were observed at a regular interval of 10 min. It was found that the system took 1–2 h to attain quasi-steady state when started from initial ambient state. However, for subsequent runs only flow rate varied and time required to attain quasi-steady state was less than 30 min. Three sets of roughened absorber plates, having $p/e = 8$, 6 and 3 had been prepared and eight values of flow rates were used for each set of test runs.

It is to be noted that, the test set up was checked by conducting experiments for a smooth duct before conducting the experiments for roughened duct. The Nusselt number and friction factor for smooth duct were determined from experimental data. These values were then compared with the values obtained from the following correlations of Dittus Boetler equation [7] for Nusselt number and with the modified Blasius equation [8] for friction factor for smooth duct:

$$Nu_s = 0.024 Re^{0.8} Pr^{0.4}, \tag{1}$$

$$f_s = 0.085 Re^{-0.25}. \tag{2}$$

The following parameters were measured:

(a) Temperature of the heated plate (t_p).
(b) Temperature of air at inlet (t_i) and outlet (t_o) of the test section.
(c) Pressure drop across the test section (ΔP).
(d) Pressure difference across the orifice-meter (ΔP_o).

2.3. Data reduction

The experimental data have been reduced to obtain the average plate temperature, average air temperature, mass flow rate and Reynolds number. These data were then used to determine the heat transfer coefficient, Nusselt number and friction factor. The theory of data reduction is discussed below.

The average plate temperature (t_p) is calculated by recording the temperatures of 15 thermocouples mounted on the absorber plate and then taking the average of it. Similarly average air temperature t_a is determined by taking the average of temperatures of thermocouples inserted into the test section duct.

The pressure difference across the orifice meter obtained from the U-tube manometer with the tilt angle (θ) of 10° has been used for the determination of mass flow rate from the equation given below:

$$m = C_d A_o \left[\frac{2\rho \Delta P_o \sin \theta}{1 - \beta^4} \right]^{0.5}. \tag{3}$$

The average heat transfer coefficient was then calculated from the following expression:

$$h = \frac{\dot{m} C_p (t_o - t_i)}{A_C (t_P - t_a)}. \tag{4}$$

The average heat transfer coefficient (h) was then used to obtain the average Nusselt number as follows:

$$Nu = \frac{h D_h}{k}. \tag{5}$$

The friction factor was determined from the measured values of pressure drop (ΔP) across the test section as given below:

$$f = \frac{2 \Delta P D_h}{4 \rho L v^2}. \tag{6}$$

3. Correlation for Nusselt number and friction factor

A statistical correlation is developed on the basis of regression analysis of the experimental data obtained. Fig. 4 shows a plot of Nusselt number as a function of Reynolds number for the entire data for a combination of rib geometry. The power law relation between Nusselt number and Reynolds number is shown below

$$Nu = B_0 \times Re^{1.213}. \tag{7}$$

The coefficient B_0 will in fact be function of other influencing parameter. The other parameter is relative roughness pitch (p/e), the value of ($Nu/(Re)^{1.213}$) has been plotted against relative roughness pitch (p/e) in Fig. 5. Finally Eq. (8) yields the following correlation for Nusselt number:

$$\frac{Nu}{Re^{1.213}} = 0.0006 \times (p/e)^{0.0104} \quad \text{and}$$

$$Nu = 0.0006 \times Re^{1.213} \times (p/e)^{0.0104}. \tag{8}$$
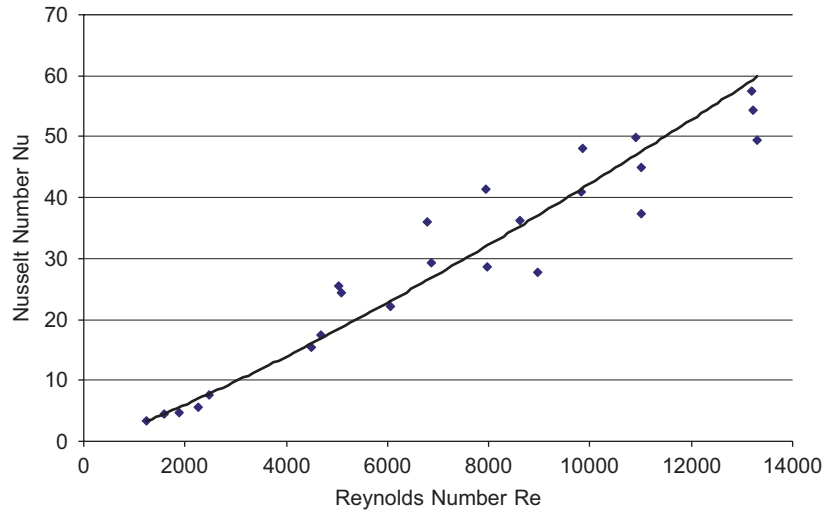
Fig. 4. Plot of Nusselt number with Reynolds number.
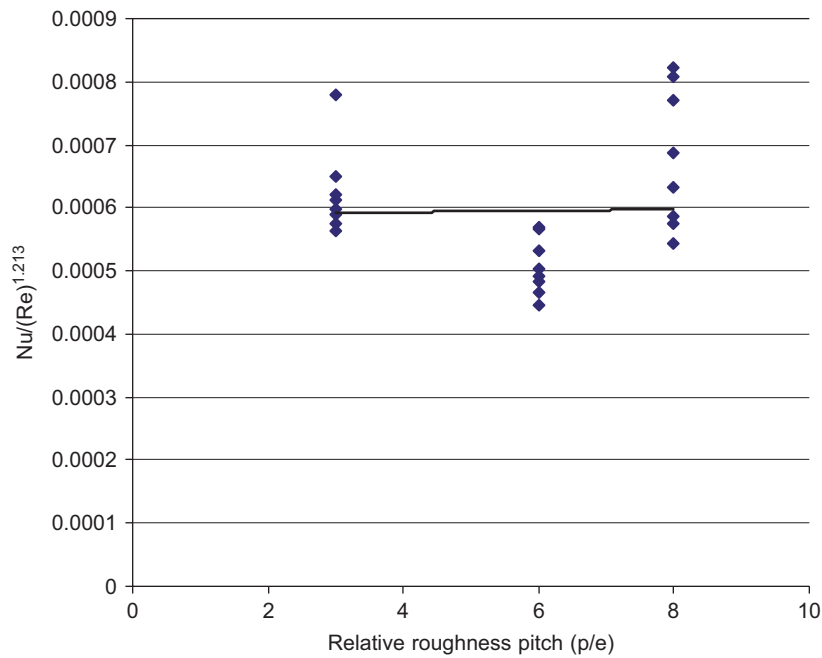
Fig. 5. Plot of $Nu/(Re)^{1.213}$ with relative roughness pitch (p/e).

A similar method has been used to develop a correlation for friction factor. Fig. 6 shows a plot of Friction factor as a function of Reynolds number for the entire data for combination of rib geometry. The power law relation between Friction factor and Reynolds number is shown below:

$$f = C_0 \times Re^{-0.3685}. \tag{9}$$

The coefficient C_0 will in fact be function of other influencing parameter. The other parameter is relative roughness pitch (p/e), the value of $f/Re^{-0.3685}$ has been plotted against relative roughness pitch (p/e) in Fig. 7. Finally Eq. (10) yields the following correlation for friction

factor:

$$\frac{f}{Re^{-0.3685}} = 1.0858 \times (p/e)^{0.0114} \quad \text{and}$$
$$f = 1.0858 \times (Re)^{-0.3685} \times (p/e)^{0.0114}. \tag{10}$$

4. Thermal performance

As per ASHRAE recommendations the thermal efficiency of a solar collector can be expressed by the following equation [6]:

$$\eta = F_R\left[(\tau\alpha) - U_L\left(\frac{t_i - t_a}{I}\right)\right], \tag{11}$$
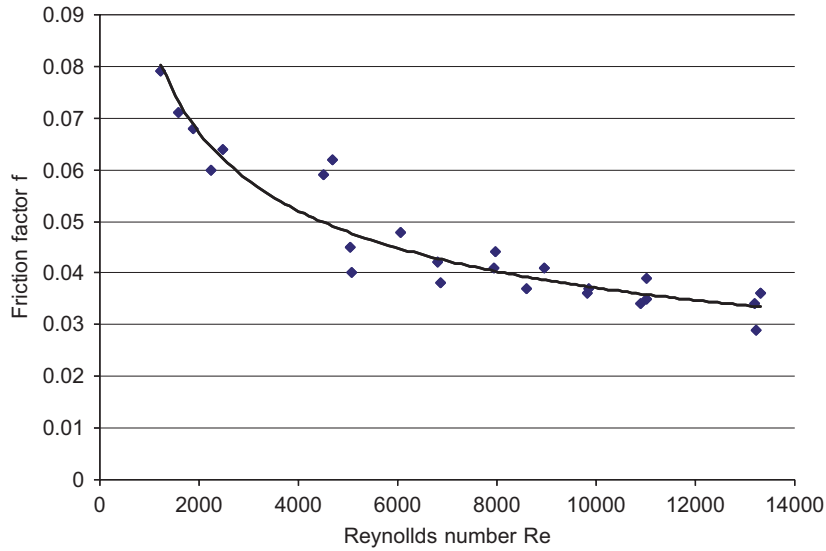
Fig. 6. Plot of friction factor with Reynolds number.
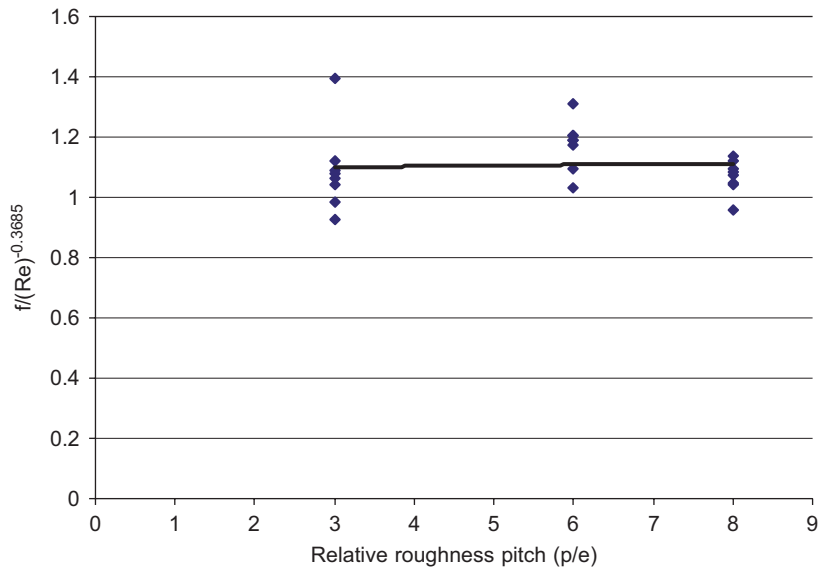
Fig. 7. Plot of $f/(Re)^{-0.3685}$ with relative roughness pitch.

where F_R is the 'collector heat removal factor' defined as the ratio of the actual heat transfer to the maximum possible rate.

The relation between the collector efficiency factor F' and the heat removal factor F_R is given as

$$F_R = \frac{mC_p}{A_C U_L}[1 - \text{Exp}(-A_C U_L F'/mC_p)]. \tag{12}$$

In a particular case of a solar air heater without recycling and where the inlet air temperature coincides the ambient (i.e., $t_i = t_a$), Eq. (11) reduces to $h = F_R(\tau\alpha)$. This expression of efficiency does not allow the real operative temperature to be shown and it, therefore, results less efficacious. In view of these limitations Biondi et al. [9] proposed the following equation for efficiency of solar air

heaters:

$$\eta = F_o\left[(\tau\alpha) - U_L\left(\frac{t_o - t_i}{I}\right)\right], \tag{13}$$

where F_o is the heat removal factor referred to the outlet temperature and can be expressed as

$$F_o = \frac{GC_p}{U_L}[\text{Exp}(U_L F'/GC_p) - 1]. \tag{14}$$

Eq. (13) indicates that a plot of efficiency against $[(t_o - t_i)/I]$ will result in a straight line whose slope is $F_o U_L$ and ordinate axis intercept is $F_o(\tau\alpha)$, if F_o, U_L and $(\tau\alpha)$ are not very strong functions of operating parameters like mass flow rate, intensity of solar radiation, ambient temperature and wind velocity variations. Further, thermal

performance can also be expressed based on temperature gain produced by the collector and expressed as

$$\eta = \frac{GC_p(t_o - t_i)}{I}. \tag{15}$$

5. Thermal performance prediction

The thermal performance of a solar air heater can also be predicted on the basis of detailed consideration of heat transfer processes in the system. Using the correlations for heat transfer coefficient and friction factor developed, and the performance parameters, namely overall heat loss coefficient, heat removal factor and other relevant factors can then be evaluated. For this purpose a step-by-step procedure has to be followed. In order to compute the values of loss coefficient and heat removal factor plate temperature are assumed and an iterative process followed to match the values of total energy gain. Subsequently, the value of effective efficiency of solar air heater can be determined. A computer program of calculation has been developed. Various steps involved in the iterative process have been explained below.

Step 1: An initial estimate for the mean absorber plate temperature t_p is made by using the approximation $t_p = t_a = t_i$.

Step 2: Using this plate temperature, top loss coefficient, U_t, and then overall loss coefficient, U_L, are computed using the following equations. The top loss coefficient U_t can be computed using the relationship proposed by Klien [10] as given below:

$$U_t = \left[\frac{N}{(349/t_p)[(t_p - t_a)/(N + \delta)]^{0.33}} + \frac{1}{h_w} \right]^{-1}$$
$$+ \frac{\sigma(t_p - t_a)(t_p^2 + t_a^2)}{[\varepsilon_p + 0.05N(1 - \varepsilon_p)]^{-1} + [(2N + \delta - 1)/\varepsilon_g] - N} \tag{16}$$

where $\delta = (1 - 0.04h_w + 0.005h_w^2)(1 + 0.091N)$.

Using this value of top loss coefficient, the overall loss coefficient can be determined from

$$U_L = U_t + \frac{k_i}{t}, \tag{17}$$

where k_i is the thermal conductivity and t is the thickness of insulating material.

Step 3: Using this estimated loss coefficient U_L, the efficiency factor F', and heat removal factor F_o are computed using the following equations. The heat removal factor, F_o, is given by

$$F_o = \frac{GC_p}{U_L}\left[\text{Exp}\left(\frac{U_L F'}{GC_p}\right) - 1\right], \tag{18}$$

where F', the collector efficiency factor can be computed from the following relation:

$$F' = \frac{h}{h + U_L}. \tag{19}$$

The heat transfer coefficient h can be determined from the correlation developed

$$h = 0.0006 \times Re^{1.213} \times (p/e)^{0.0104} \frac{k}{D_h}. \tag{20}$$

Net thermal energy gain is then computed using the following equation:

$$q_u = A_c[I(\tau\alpha) - U_L(t_p - t_a)]. \tag{21}$$

The temperature rise is computed using the equation given below:

$$(t_o - t_i) = \frac{q_u}{mC_p}. \tag{22}$$

Step 4: These estimates for heat removal factor F_o, loss coefficient U_L, heat energy gain q_u, and temperature rise $(t_o - t_i)$ are then used in the following equation to compute the new mean plate temperature:

$$t_p = t_a + F_o I(\tau\alpha)\left[\frac{1 - F_o}{F_o U_L} + \frac{t_o - t_i}{I(\tau\alpha)}\right]. \tag{23}$$

Step: 5 This new mean plate temperature is compared with the previous value and the difference decides the further course of calculations. If difference is within acceptable limits, the process is terminated while if the difference is outside the tolerance limits the calculated value of t_p is used as revised value.

Step 6: Using this revised value of mean plate temperature the above steps (1–5) are repeated till new and old values of mean plate temperature agree within specified limits.

Step 7: When the correct plate temperature has been determined from this iterative procedure, the thermal efficiency of solar air heater is calculated by using the following expression:

$$\eta = F_o\left[(\tau\alpha) - U_L\left(\frac{t_o - t_i}{I}\right)\right]. \tag{24}$$

By using this procedure the thermal efficiency is estimated and compared the results with the experimental data obtained.

6. Results and discussions

The performance for solar air heaters with different roughness and operating parameters have been evaluated and presented in Fig. 8. The corresponding performance for the smooth collectors has also been shown in Fig. 8. The performance lines have been drawn for three values of (p/e) and one for smooth absorber plate. Results show that the roughened collector with absorber plate having relative roughness pitch (p/e) of 8 gives the best performance.

The experimental and the predicted values of the thermal efficiency for the roughened duct are presented in Fig. 9. This plot shows that the deviation is ±12% which is, fairly in acceptable limits. It is therefore recommended that the proposed procedure can be successfully employed for predicting the solar collector performance.
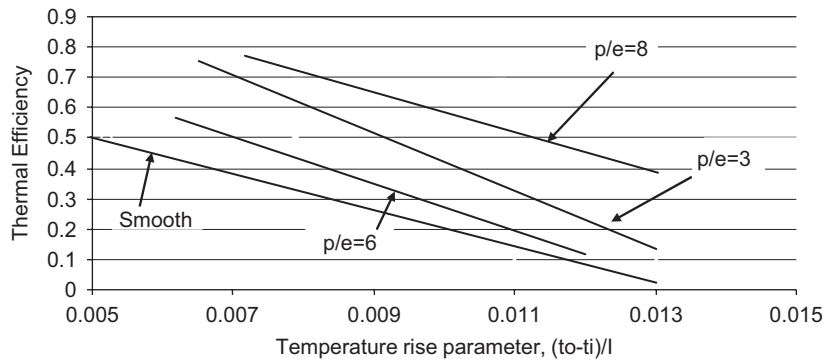
Fig. 8. Effect of relative roughness pitch on thermal performance.
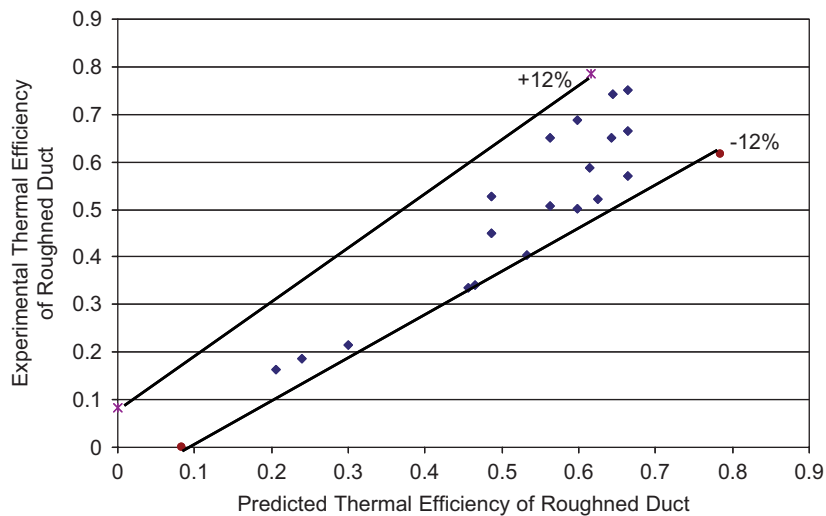
Fig. 9. Experimental versus predicted thermal efficiency of roughened duct.

7. Conclusions

The present work was undertaken with the objective of detailed investigation of roughness geometries that have a combination of transverse as well as inclined ribs. Results have been compared with those of a smooth duct under similar flow conditions to determine heat transfer coefficient and friction factor. The thermal performance of roughened solar air heater is influenced by the roughness parameters and the best performance has been found for the roughness parameter that yield maximum heat transfer coefficient. The geometry having relative roughness pitch of 8 have the maximum thermal efficiency. The analytical determination of thermal performance of roughened solar air heater has been carried out. It is concluded that the proposed procedure can be successfully employed for predicting the solar air heater performance.

References

[1] Bhagoria JL, Saini JS, Solanki SC. Heat transfer coefficient and friction factor correlations for rectangular solar air heater duct having transverse wedge shaped rib roughness on the absorber plate. Renew Energy 2002;25:341–69.

[2] Prasad K, Mullick SC. Heat transfer characteristics of a solar air heater used for drying purpose. Appl Energy 1985;12: 83–93.

[3] Webb RL. Heat transfer and friction in tubes with repeated rib roughness. Int J Heat Mass Transfer 1971;14:601–17.

[4] Prasad BN, Saini JS. Effect of artificial roughness on heat transfer and friction factor in solar air heater. Sol Energy 1988;41: 555–60.

[5] Varun, Saini RP, Singal SK. A review on roughness geometry used in solar air heaters. Sol Energy 2007, in press.

[6] ASHRAE Standards 93-77. Methods of testing to determine the thermal performance of solar collectors. New York;1977.

[7] Kays WH, Perkin H. Forced convection internal flow in ducts. In: Rohsenow WM, Harnett IV, editors. Handbook of heat transfer. New York: McGraw Hill; 1990.

[8] Bhatti MS, Shah RK. Turbulent and transition convective heat transfer in ducts. In: Kakac S, Shah RK, Aung W, editors. Handbook of single phase convective heat transfer. New York: Wiley; 1987. p. 4.1–4.166.

[9] Biondi P, Cicala L, Farina G. Performance analysis of solar air heaters of conventional design. Sol Energy 1988;41(1):101–7.

[10] Klien SA. Calculation of flat plate loss coefficients. Sol Energy 1975;17:79.